project.docx



Delhi Technological University

Document Details

Submission ID

trn:oid:::27535:102559286

Submission Date

Jun 26, 2025, 2:21 PM GMT+5:30

Download Date

Jun 26, 2025, 2:28 PM GMT+5:30

File Name

project.docx

File Size

7.2 MB

39 Pages

8,220 Words

47,917 Characters



9% Overall Similarity

The combined total of all matches, including overlapping sources, for each database.

Filtered from the Report

- Bibliography
- Quoted Text
- Cited Text
- Small Matches (less than 10 words)

Match Groups



43 Not Cited or Quoted 9%

Matches with neither in-text citation nor quotation marks



99 0 Missing Quotations 0%

Matches that are still very similar to source material



0 Missing Citation 0%

Matches that have quotation marks, but no in-text citation



0 Cited and Quoted 0%

Matches with in-text citation present, but no quotation marks

Top Sources

Internet sources

Publications

Submitted works (Student Papers)

Integrity Flags

0 Integrity Flags for Review

No suspicious text manipulations found.

Our system's algorithms look deeply at a document for any inconsistencies that $% \left(1\right) =\left(1\right) \left(1\right) \left($ would set it apart from a normal submission. If we notice something strange, we flag it for you to review.

A Flag is not necessarily an indicator of a problem. However, we'd recommend you focus your attention there for further review.





Match Groups

43 Not Cited or Quoted 9%

Matches with neither in-text citation nor quotation marks

99 0 Missing Quotations 0%

Matches that are still very similar to source material

0 Missing Citation 0%

Matches that have quotation marks, but no in-text citation

• 0 Cited and Quoted 0%

Matches with in-text citation present, but no quotation marks

Top Sources

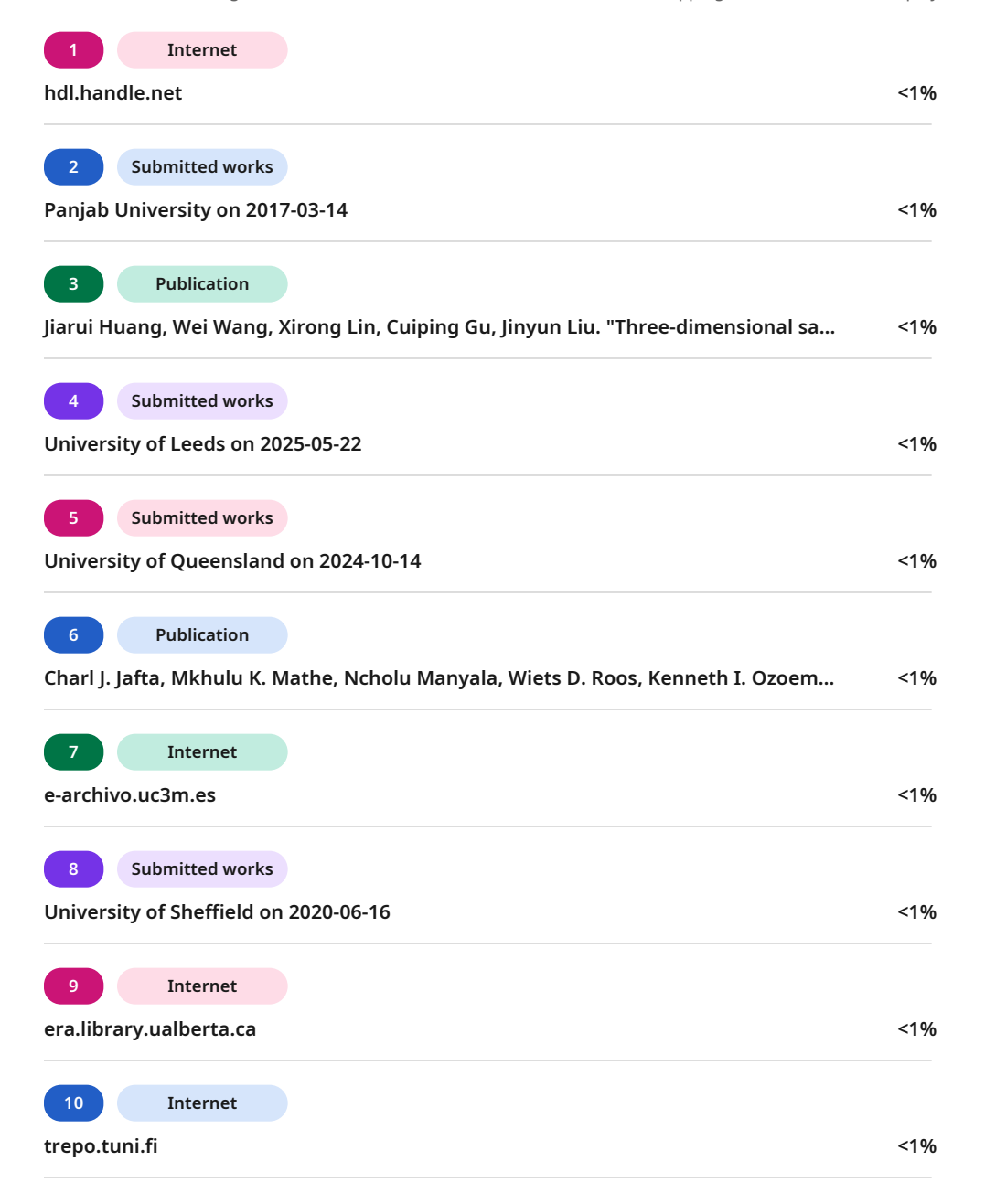
6% Internet sources

5% Publications

6% Land Submitted works (Student Papers)

Top Sources

The sources with the highest number of matches within the submission. Overlapping sources will not be displayed.







11	Internet		
busines	ssdocbox.com		<1%
12	Submitted works		
Indian i	Institute of Techn	ology, Madras on 2017-06-06	<1%
13	Submitted works		
Nanyar	ng Technological L	Jniversity, Singapore on 2013-03-27	<1%
14	Submitted works		
New Yo	ork Institute of Ted	chnology on 2024-04-10	<1%
15	Submitted works		
Univers	sity of Malaya on 2	2020-04-12	<1%
16	Submitted works		
Gyeong	ısang National Un	iversity on 2020-08-11	<1%
17	Internet		
mail.wj	aets.com		<1%
18	Submitted works		
Adelaid	le High School on	2018-11-12	<1%
19	Submitted works		
Associa	tie K.U.Leuven on	2020-06-09	<1%
20	Publication		
Junshai	n Li, Xijun Xu, Xiad	oting Yu, Xu Han et al. "Monodisperse CoSn and NiSn Nan	<1%
21	Publication		
Kedong	្រ Song, Yuting Hua	ang, Xing Liu, Yunhong Jiang, Ping Zhang, Yanhuai Ding	<1%
22	Submitted works		
Univers	sity of Glasgow on	2024-04-26	<1%
23	Submitted works		
Univers	sity of Warwick on	2015-03-11	<1%
24	Internet		
ijsrst.co	om		<1%





25 Internet	
www.frontiersin.org	<1%
Transmitted in the control of the co	
26 Internet	~10 /
www.mdpi.com	<1%
27 Publication	
Gharibi, H "Effect of polyaniline-doped trifluoromethane sulfonic acid nanofiber	<1%
28 Publication	
Huimin Li, Jiahuan Li, Arne Thomas, Yaozu Liao. " Ultra-High Surface Area Nitroge	<1%
29 Publication	
	~10 6
S. Harikrishnan, A. R. Abhijith, Jyoti Rajput, Deepak Sharma, Amar Srivastava. "ch	<1%
30 Submitted works	
Universiti Malaysia Pahang on 2015-05-06	<1%
31 Submitted works	
University of Sheffield on 2019-05-16	<1%
32 Internet	
d-nb.info	<1%
u-no.into	~170
33 Internet	
eprints.lancs.ac.uk	<1%
34 Internet	
oa.upm.es	<1%
35 Internet	
pubs.rsc.org	<1%
36 Publication	
Haifa Zhai, Yuge Zhao, Zhehong Liu, Fuming Zhang, Min Du, Zhitao Wang, Gongk	<1%
37 Publication	
Huan Yang, Chih-Yao Chen, Jinkwang Hwang, Keigo Kubota, Kazuhiko Matsumoto	<1%
38 Internet	
dr.iiserpune.ac.in:8080	<1%





39	Internet
journal.b	crec.id
40	Internet
pluginhig	hway.ca
41	Internet
powering	autos.com
42	Internet
wrap.war	wick.ac.uk





Chapter 1 INTRODUCTION

1.1 Rechargeable Batteries

Rechargeable batteries, also known as secondary batteries, are energy storage devices that can be repeatedly charged and discharged, unlike primary (non-rechargeable) batteries [1]. Their ability to efficiently store and deliver electrical energy makes them essential for a variety of applications, from electrical to energy storage technologies. The evolution of rechargeable battery technology has been driven by the increasing demand for higher energy density, longer cycle life, improved safety, and lower cost [2-3].

Traditionally, several types of rechargeable batteries have played significant roles:

- Lead-Acid Batteries: The Lead-Acid based rechargeable battery are known for their robustness, low cost, and ability to deliver high surge currents, making them suitable for automotive starting, lighting, and ignition (SLI) applications, as well as uninterruptible power supplies (UPS) [4]. However, their relatively low energy density and environmental concerns regarding lead disposal limit their application in portable devices [5].
- Nickel-Cadmium (Ni-Cd) Batteries: Developed in the early 20th century, Ni-Cd batteries offered better energy density and cycle life compared to lead-acid [6]. They are widely used in many applications. A major drawback is the "memory effect," where repeated partial discharge cycles can lead to a reduction in capacity. Furthermore, cadmium is a highly toxic heavy metal, leading to their phasing out in many regions [7-8].
- Nickel-Metal Hydride (Ni-MH) Batteries: The Ni-MH based-batteries were first replaced as a more green alternative solution to Ni-Cd batteries in the late 1980s. Ni-MH batteries



have a higher energy density than Ni-Cd and exhibit a less pronounced memory effect [9]. While an improvement, their energy density and voltage are still lower than those of lithiumion batteries [10].

- Lithium-Ion Batteries (LIBs): Emerged in the early 1990s and revolutionized portable electronics due to their high energy density, high operating voltage, and absence of memory effect [11]. They quickly became the dominant technology for smartphones, laptops, and more recently, electric vehicles (EVs) and energy storage devices. Their continuous development aims to enhance safety, further increase energy density, extend cycle life, and reduce cost [12-13].
- Other Emerging Technologies: Research and development are ongoing for various next-generation battery technologies, including solid-state batteries, lithium-sulfur (Li-S) batteries, lithium-air (Li-air) batteries, and sodium-ion (Na-ion) batteries, which aim to surpass the performance limitations of current Li-ion technology in terms of energy density, safety, and cost [14-15].

Each type of rechargeable battery possesses unique characteristics which dictate their suitability for specific applications.

1.2 Lithium-Ion Batteries (LIBs)

Lithium-Ion Batteries (LIBs) represent the leading edge of current rechargeable battery technology, dominating the market for a vast range of applications due to their superior energy and power characteristics [16]. Their success stems from the high electrochemical potential of lithium and its ability to reversibly diffuse into various electrode materials [17-18].

1.2.1 Components of LIBs

A typical LIB cell consists of four main components as electrolyte, cathode, separator, and anode.

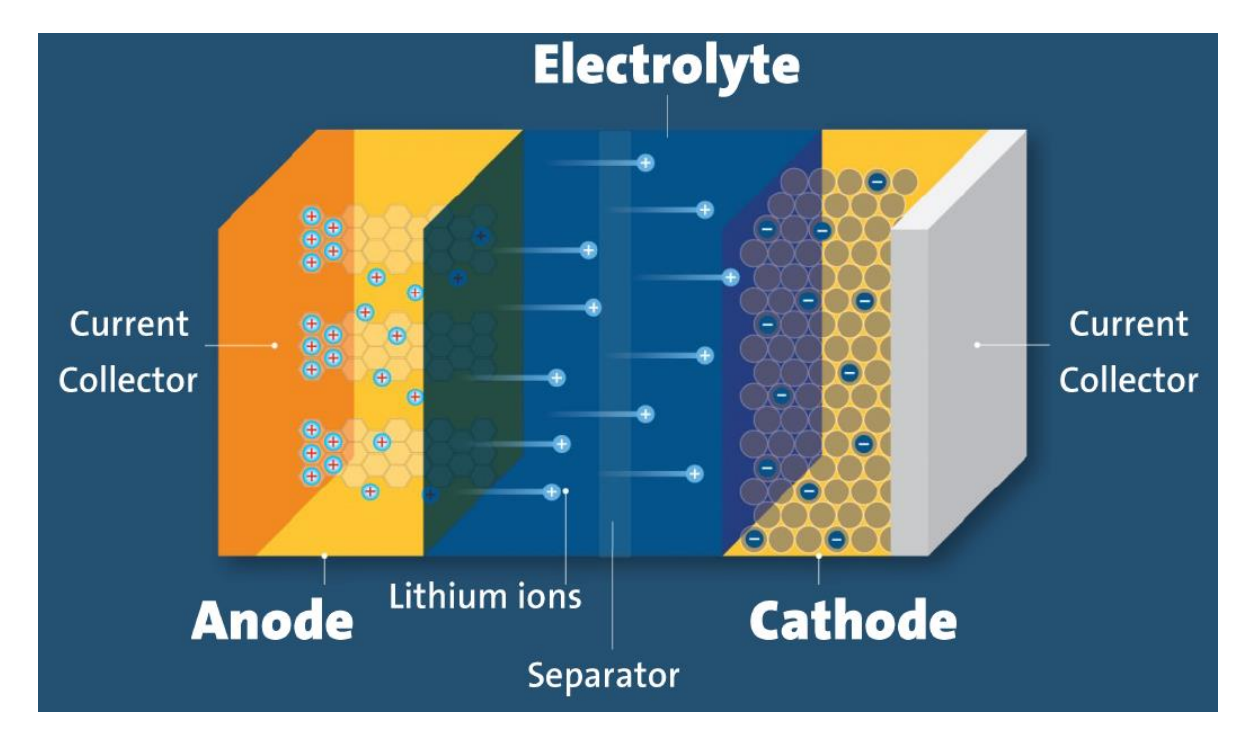


Fig. 1: Components of Lithium-Ion Battery

1.2.1.1 Electrolyte

The electrolyte facilitates the transport of lithium ions (Li⁺) from anode to cathode and vice versa. It must possess high ionic conductivity and electronic insulation. The most common type of electrolyte in commercial LIBs is a non-aqueous solution consisting of lithium salts dissolved in organic solvents [19-20].

- Lithium Salts: The widely used lithium salt is lithium hexafluorophosphate (LiPF₆) because of its conductivity, stability, and ability for the formation of stable SEI. Other salts like lithium bis(trifluoromethanesulfonyl)imide (LiTFSI) and lithium bis(oxalato)borate (LiBOB) are also explored for specific properties like enhanced safety or improved high-temperature performance [21].
- Organic Solvents: Common organic solvents include cyclic carbonates and linear carbonates. Ethylene carbonate (EC) is crucial for forming a stable SEI layer, while Dimethyl carbonate (DMC) is often added to lower viscosity and improve ionic conductivity. The mixture of these solvents is carefully optimized to achieve a balance of properties [22].



• Additives: Small amounts of additives are often included to improve specific aspects of battery performance, such as enhancing SEI formation, improving high-voltage stability, or acting as flame retardants [23].

1.2.1.2 Cathode

The cathode (positive electrode) is typically a lithium-containing metal oxide. This material releases lithium ions when the battery discharges and restores them when it charges. Key requirements for cathode materials include high specific capacity, high operating voltage, good cycle stability, and thermal stability [24].

Common cathode materials include:

- Lithium Cobalt Oxide (LiCoO₂, LCO): It is known for its high energy density and relatively simple synthesis. It is widely used in portable electronic devices (smartphones, laptops) but suffers from limited thermal stability and cycle life, especially at high charge rates, and contains expensive cobalt [25].
- Lithium Manganese Oxide (LiMn₂O₄, LMO): A spinel structure material offering good thermal stability and lower cost. It has a high power capability but typically lower specific capacity compared to LCO and can suffer from manganese dissolution at elevated temperatures [26].
- Lithium Nickel Manganese Cobalt Oxide (LiNiMnCoO₂, NMC): A ternary blend that combines the advantages of nickel (high capacity), manganese (stability, lower cost), and cobalt (stability, power). By varying the ratios of Ni, Mn, and Co, properties can be tuned for various applications. NMC is a dominant material in electric vehicles [27].
- Lithium Iron Phosphate (LiFePO₄, LFP): Characterized by its exceptional thermal stability, long life, and low cost. Although its operating voltage is lower than other cathode



materials, leading to slightly lower energy density, its safety and longevity make it ideal for power tools, electric buses, and grid-scale energy storage [28].

Table 1: Analysis of cathode materials

Material	Theoretical Specific Capacity (mAh g ⁻¹)	References
LiCoO ₂	274	[25]
LiMn ₂ O ₄	148	[26]
LiNiMnCoO ₂	150-200	[27]
LiFePO4	170	[28]
LiMgMnO ₄	160-170	[29]
LiNiO ₂	275	[30]

1.2.1.3 Separator

The separator a porous membrane that is placed between the anode and cathode for allowing the free flow of lithium ions through the electrolyte and to prevent electronic short-circuiting. It must be electronically insulating, chemically stable within the electrolyte, mechanically strong, and have good wettability with the electrolyte [31].

- Materials: Typically made from polymer materials such as polyethylene (PE) or multilayered PE/PP structures. These materials are chosen for their chemical inertness and low cost.
- **Pore Structure**: The separator has a precise pore structure that allows for optimal ion transport and to prevent short-circuiting.



1.2.1.4 Anode

The anode (negative electrode) is the host material for lithium ions. During charging, commonly known as intercalation these ions are stored in the anode material and released during discharging, commonly known as de-intercalation. The ideal anode material should have high specific capacity, good cycle stability, low volume expansion upon lithiation, and a safe operating potential close to that of metallic lithium.

- **Graphite:** The most common anode material is Graphite is favoured due to its excellent electrical conductivity, good cycling performance, relatively low cost, and relatively low volume change during lithium intercalation. Lithium ions insert into the layered structure of graphite to form LiC₆ [32].
- Silicon (Si): Silicon has a theoretical specific capacity significantly higher than graphite.

 This high capacity makes silicon a promising next-generation anode material. However, it suffers from large volume changes, leading to mechanical degradation and rapid capacity fade. Research focuses on silicon or combining it with graphite to mitigate these issues [33].
- Lithium Titanate (Li₄Ti₅O₁₂, LTO): A spinel oxide material known for its exceptional cycle life because of its "zero-strain" intercalation mechanism. However, its higher operating potential leads to a lower cell voltage and thus lower energy density compared to graphite anodes. LTO is used in applications requiring long life and high safety, such as electric buses and energy storage systems [34].



Table 2: Analysis of different anode materials

Material	Theoretical Specific Capacity (mAh g ⁻¹)	References
Graphite	960	[32]
Silicon	4200	[33]
Porous Carbon	800-1000	[35]
Carbon Nanotubes	1100	[36]
SiO	1600	[37]
Transition Metal Oxides	500-1200	[38]

1.3 Principle and Working

The working principle of a LIB relies on the reversible diffusion of lithium ions into and out of the electrode materials. This process does not involve the formation of metallic lithium, hence the term "Lithium-Ion Battery" [39].

1.3.1 Electrochemistry

During discharge (when the battery provides power), ions de-intercalate from the anode and intercalate into the cathode material by passing through the electrolyte and separator. Simultaneously, electrons are released from the anode, flow through the external circuit, and reenter the cathode to balance the charge [40].

Anode reaction for Graphite:

$$Li_{x}C_{6} \rightleftharpoons x Li^{+} + x e^{-} + 6 C \tag{1}$$

18

vii



Cathode reaction for LCO:

$$\text{Li}_{1-x}\text{CoO}_2 + x \text{Li}^+ + x \text{ e}^- \rightleftharpoons \text{LiCoO}_2$$
 (2)

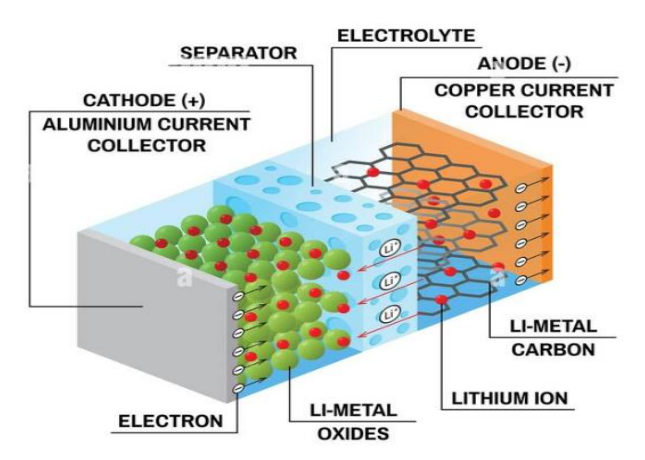


Fig. 2: Dis-charging process in LIBs

During charging, the external power source reverses the process. The ions de-intercalate from the cathode, migrate back and intercalate into the anode material. Electrons flow from the cathode through the external circuit to the anode [41].

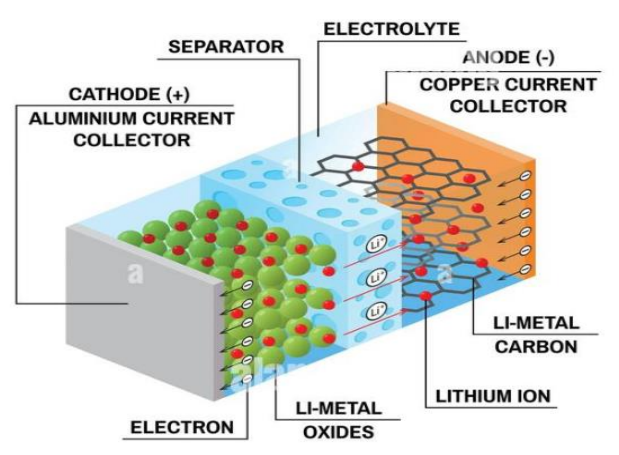


Fig. 3: Charging process in LIBs

For typical LIBs, the average operating voltage is around 3.7 V [42]. The overall electrochemical reaction for a LIB cell can be represented as:

Overall Reaction (Discharge):

$$\text{Li}_{x}\text{C}_{6} + \text{Li}_{1-x}\text{CoO}_{2} \rightarrow 6 \text{ C+ LiCoO}_{2}$$
 (3)

1.3.2 Electrochemical Performance

The performance of a LIB is characterized by several key metrics [43]:

viii





1.3.2.1 Charge/Dis-charge

- Charge Cycle: The process of supplying electrical energy to the battery to restore its stored chemical energy.
- **Discharge** Cycle: The process of the battery releasing its stored chemical energy as electrical energy.
- C-rate: The rate at which a battery is charged or discharged with relation to its maximum capacity of the active material. Lower C-rates gives the structural stability of the electrode material whereas higher C-rates generally lead to reduced effective capacity.

1.3.2.2 Specific Capacitance

Specific capacitance refers to the capability of a material to store electrical charge in relation to its unit mass, usually expressed in Farads per gm (F g⁻¹).

Specific capacity is the measurement of the maximum amount of electrical charge that can be stored in relation to its unit mass, stated as milliampere-hours per gram (mAh g⁻¹). It is a crucial parameter for determining the energy density of a battery [44].

1.3.2.3 Lithium-Ion Diffusion Coefficient

It quantifies the rate of diffusion of lithium ions to move through electrode-electrolyte interface. A higher diffusion coefficient indicates faster ion transport, which is critical for achieving high power density and efficient charge/discharge at high C-rates [45]. The kinetics of lithium ion transport through solid electrodes is taken as the rate-determining step. Various electrochemical techniques, such as Electrochemical Impedance Spectroscopy (EIS), Cyclic Voltammetery (CV) and Galvanostatic Intermittent Titration Technique (GITT), are used to determine the diffusion coefficients [46-47].





Chapter 2

LITERATURE REVIEW

This chapter gives a conceptual idea of existing literature pertinent for characterization of electrode materials for energy storage applications. A particular focus is placed on various types of anode materials, their electrochemical mechanisms, and their performance characteristics.

2.1 Types of Anodes

Anode materials are critical components in LIBs for enhanced electrochemical performance. The selection of an anode material is crucial as it significantly dictates the overall energy density and long-life cycle of the device. This section reviews prominent categories of anode materials [48].

Intercalation-Type Anodes

Intercalation-type anodes store lithium ions reversibly within their layered structures without undergoing significant structural changes or forming new chemical bonds with the host material. The lithium ions insert themselves into vacant sites or interstitial spaces within the host lattice in the charging and subsequently extracted out in the discharging process. This "rocking-chair" mechanism, where lithium ions shuttle between the anode and cathode, relies on the structural integrity of the host material [49]. For example, Graphite.

The general reaction for an intercalation anode (M) is represented as:

$$M + x Li^{+} + x e^{-} \rightleftharpoons Li_{x}M \tag{4}$$

During lithiation, lithium ions and electrons are simultaneously inserted into the host lattice. During delithiation, they are extracted. The process is typically reversible, leading to good cycling stability.

Alloying-Type Anodes





Alloying-type anodes store lithium ions through a reversible alloying reaction, where lithium combines with the electrode material, forming a distinct lithium-rich alloy phase. This mechanism typically involves a high number of lithium ions per host atom, leading to significantly higher theoretical specific capacities than intercalation-type materials [50]. For example, Silicon.

The general reaction for an alloying anode (M) represented as:

$$M + x Li^{+} + x e^{-} \rightleftharpoons Li_{x}M_{alloy}$$
 (5)

During lithiation, the host material alloys with lithium to form a Li_xM phase, undergoing a phase transformation. During de-lithiation, the alloy phase de-alloys, releasing lithium ions and typically returning to the original host material or a stable intermediate phase.

Conversion-Type Anodes

Conversion-type anodes store lithium ions via a reversible conversion reaction, where the host material (typically a metal oxide, sulfide, phosphide, or nitride) is fully decomposed into metallic nanoparticles and an amorphous lithium compound (e.g., Li₂O, Li₂S, Li₃P). This mechanism involves the breaking of existing bonds and the formation of new ones, typically involving multi-electron transfer, which contributes to very high theoretical capacities [51]. For example, Transition Metal Oxides (TMOs).

The general conversion reaction for a metal oxide (M_xO_y) in a LIBs can be represented as:

$$M_xO_y + 2 yLi^+ + 2 ye^- \rightleftharpoons xM + yLi_2O$$
 (6)

During lithiation, the metal oxide is reduced to finely dispersed metallic nanoparticles (M) embedded within an amorphous Li₂O matrix. Upon de-lithiation, the reverse oxidation reaction occurs, ideally regenerating the original metal oxide.

2.1.1 Transition Metal Oxides (TMOs)



TMOs have garnered significant attention as anode materials. Unlike traditional graphite anodes that primarily rely on intercalation mechanisms, many TMOs operate via a conversion reaction mechanism. This involves the reversible breaking and reforming of metal-oxygen bonds during the charge and discharge processes [52].

Table 3: Common TMO anodes along with their advantages and di-advantages

TMOs	Advantages	Dis-advantages	Ref.
Cobalt Oxide	high theoretical	volume changes during cycling and capacity	[53]
(Co ₃ O ₄ , CoO)	capacities	fade	
Nickel Oxide	high theoretical	large volume expansion and poor electrical	[54]
(NiO)	capacities	conductivity	
Iron Oxide	low cost and	moderate cycling stability due to volume	[55]
(Fe ₂ O ₃ , Fe ₃ O ₄)	economically cheap	changes	
Manganese Oxide	high theoretical	intrinsic poor electrical conductivity and rate	[56]
(MnO ₂ , Mn ₃ O ₄)	capacities	capability	

Despite their high theoretical capacities, practical application of TMOs as anodes faces several challenges:

- Large Volume Change: The conversion reaction often involves substantial volume expansion and contraction, leading to mechanical degradation.
- **Poor Electrical Conductivity:** Most TMOs are semiconductors or insulators, resulting in high internal resistance and limited rate capability.
- Solid Electrolyte Interphase (SEI): Repeated volume changes can continuously break and reform the SEI layer, consuming active lithium and leading to irreversible capacity loss.

2.1.2 Mixed Transition Metal Oxides (MTMOs)





Mixed transition metal oxides (MTMOs), also known as complex or composite transition metal oxides, are materials composed of two or more different transition metal cations in a single oxide lattice. [57] These materials are emerging as promising anode material because of their ability to combine the advantages of individual TMOs while often mitigating their respective drawbacks. The presence of multiple metal centres can lead to enhanced electrochemical activity, improved structural stability, and superior electronic conductivity as compared with single TMOs. The synergistic effect happening between the different metal ions contribute to their improved electrochemical performance.

MTMOs primarily operate by a conversion reaction mechanism to single TMOs, but the involvement of multiple metal species adds complexity and offers potential for superior performance [58-59].

The presence of multiple metal cations can lead to enhanced lithium storage sites, Improved electrical conductivity, and better structural integrity.

Among them, compounds with the general formula AB₂O₄, exhibiting a spinel-structured within Fd3m space group, have gained attention [60]. In these materials, A cation occupies tetrahedral sites and B cation occupies octahedrally sites, both coordinated by oxygen atoms, allowing efficient lithium-ion diffusion pathways. The coexistence of two distinct transition metals in the single-phase crystal structure enables multiple redox couples, thereby improving the specific capacity, rate capability, and cyclic stability of the anode material [61-62].

2.1.2.1 Nickel Manganese Oxide (NiMn₂O₄)

Among the various MTMOs, a spinel AB₂O₄-type material, NMO (NiMn₂O₄) ia widely used as an active anode material. This is primarily due to the advantageous combination of nickel's high theoretical capacity and manganese's lower cost, environmental benignity, and relatively stable



redox chemistry. The mixed valence states of Ni and Mn, along with their different ionic radii, contribute to a complex structure that can potentially offer improved performance [63-64].

Structure

A spinel AB₂O₄-type structure of NMO where Ni cation occupies tetrahedral sites and Mn cation occupies octahedrally sites, both coordinated by oxygen atoms.

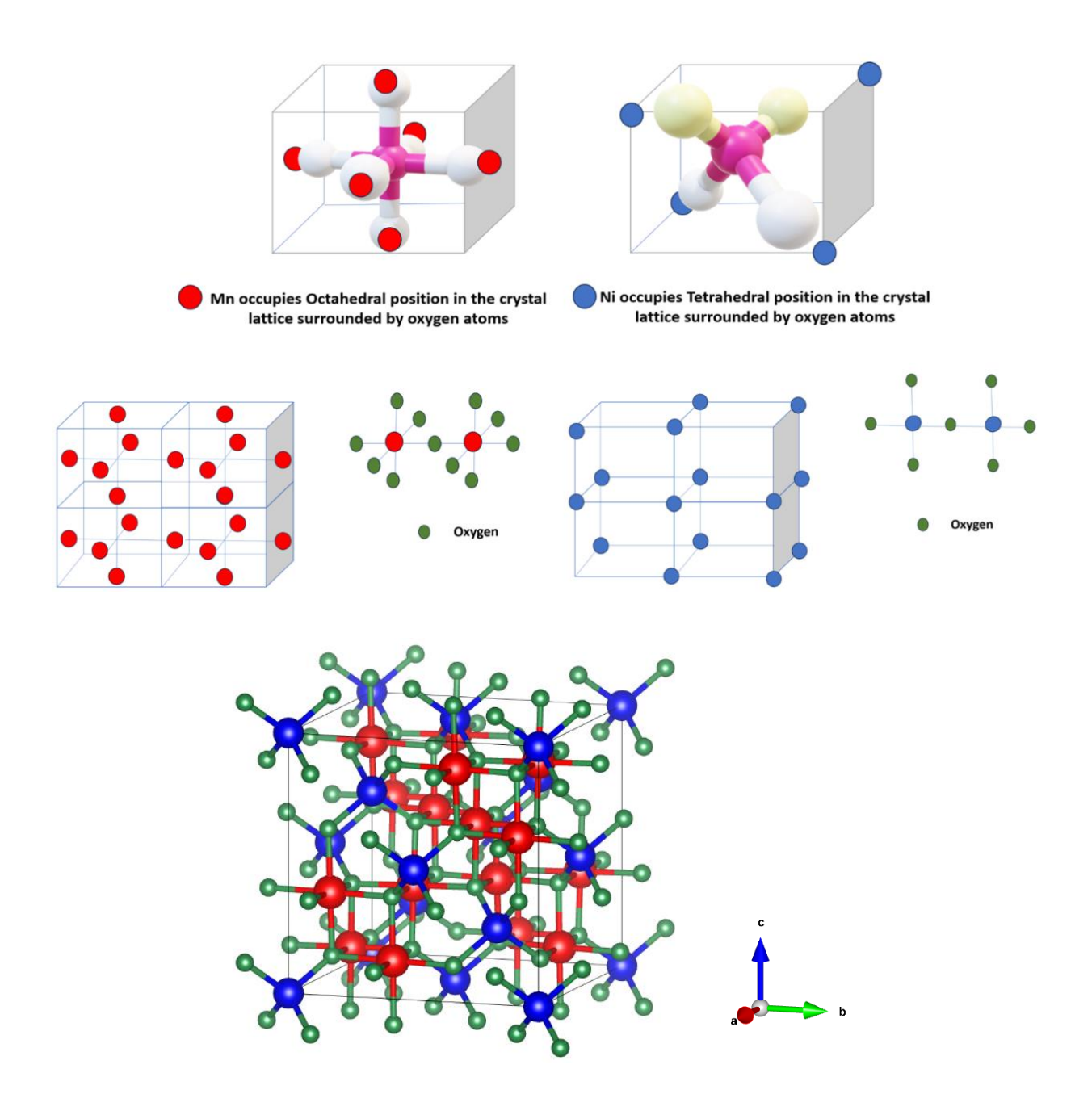


Fig. 3: Structural analysis of NMO



Mechanism

In a typical reaction for NiMn₂O₄:

$$NiMn_2O_4 + 8 Li^+ + 8 e^- \rightarrow Ni + 2 Mn + 4 Li_2O$$
 (7)

$$Ni + Li2O \rightarrow NiO + 2 Li^{+} + 2 e^{-}$$
 (8)

$$Mn + Li_2O \rightarrow MnO + 2 Li^+ + 2 e^-$$
 (9)

$$2 MnO + Li2O \rightarrow Mn3O4 + 3 Li+ + 2 e-$$
 (10)

During lithiation, both Ni and Mn ions are reduced, forming metallic Ni and Mn particles in a Li₂O matrix. During de-lithiation, the reverse oxidation of Ni and Mn occurs. The variable oxidation states of Ni and Mn, and their interplay contribute to the overall charge storage capacity. The manganese help to stabilize the structure during repeated volume changes, while nickel contributes significantly to the capacity. However, this process can also lead to structural instability, as the material undergoes changes in phase and oxidation and oxidation state [65]. These transformations can induce volume changes in the electrode, which may contribute to capacity fading and reduced cycling stability over time. On the other hand, insertion process occurs within the voids and interstitial spaces of the cubic NMO structure, where lithium ions are reversibly inserted and extracted [66-67]. This process is typically more structurally stable, though it may offer lower capacity than conversion reactions.

Both the processes contribute significantly to the overall performance of the NMO electrode during cycling. An important factor influencing these processes is the lithium-ion diffusion, which quantifies the movement or flow of lithium ions within the electrode. This coefficient is crucial for understanding the efficiency, conductivity and performance of the material during cycling and is calculated through electrochemical analysis [68-70].



Chapter 3

EXPERIMENTAL PROCEDURE

This chapter gives an outline the materials utilized for synthesizing NiMn₂O₄ as anode material and fabricating Lithium-half cell for LIBs. It covers all the structural, morphological, and electrochemical analysis for the characterization of the electrode material and fabricated electrode.

3.1 Materials and Methods

Nickel (II) acetate tetrahydrate (≥99%) and Manganese (II) acetate tetrahydrate (≥99%) were brought from Merck, India. Citric Acid (≥99%) was purchased from Thermo–Fischer Scientific, India. All the chemicals used without purification.

The precursors of Nickel and Manganese, along with Citric acid were weighed properly. A stoichiometric amount of Ni and Mn precursors were used in the ratio of 1:2. The ratio of chelating agent was kept 1:1 with the total metal ions. The simple hand grinding (solid-state) method was used to synthesis NMO. All the precursors along with chelating agent were hand grinded using mortar-pestle for around 8 hours. After grinding the sample, it was calcinated for 3 hours in a furnace at 800°C.



Fig. 5: Schematic representation of synthesis process



xvi

3.2 Material Characterization

The crystallinity and phase of the sample was analysed by XRD. The crystallite size of synthesised NMO was measured by using Scherrer equation and Williamson-Hall (W-H) plot approach, further analysed by SAED. The morphology and average particle size of the synthesised NMO was studied by SEM and TEM, and elemental mapping of synthesized sample were determined by EDS.

3.2.1 X-ray Diffraction (XRD)

XRD is a analytical technique used to identify the structural characteristics of the materials. The principle is based on the constructive interference of x-rays (x-ray of single wavelength) with a sample. When these incident x-rays strike a crystal lattice, they get diffracted at specific angles that are calculated as per Bragg's Law:

$$n\lambda = 2d\sin\Theta \tag{11}$$

In a typical setup, x-rays are generated from commonly Cu k α radiation, and then directed towards the crystalline sample. The sample is mounted on a goniometer, which precisely controls the angle of incidence (θ) and the angle of detection (2θ). As the sample rotates, different crystallographic planes satisfy Bragg's Law, leading to diffracted beams of varying intensities. XRD provides data on the phase identification of crystalline materials, lattice parameters, and crystallite size.

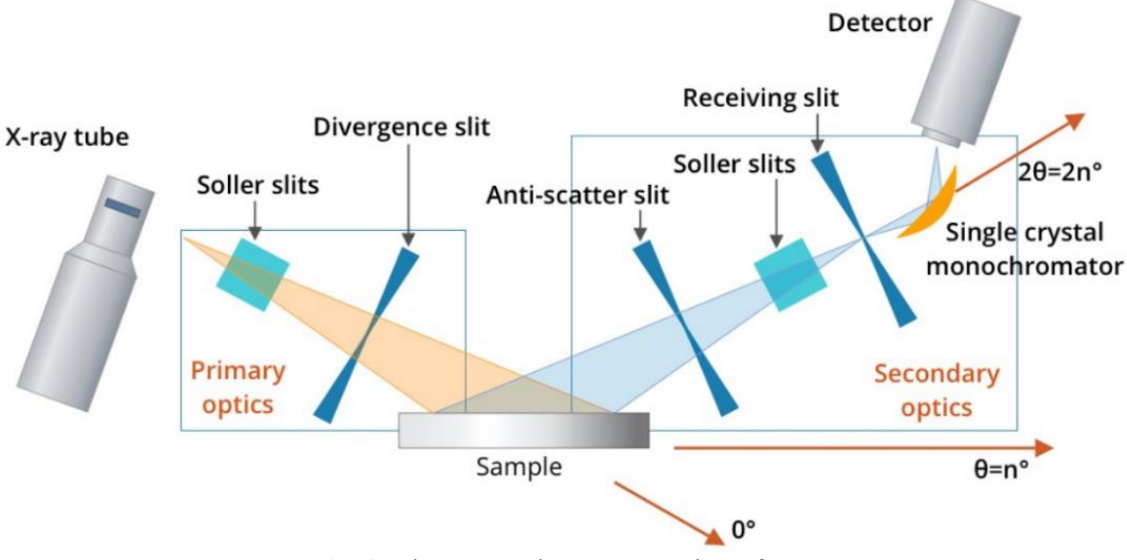


Fig 6: Diagrammatic representation of XRD

xvii



34

3.2.2 Scanning Electron Microscopy (SEM)

SEM is a technique that produces high-resolution images at micro- to nano-meter scale of the surface of the sample, by bombarding it with a finely focused beam of electrons. When the incident electron beam interacts with the sample, various signals are produced, including secondary electrons (SEs), backscattered electrons (BSEs), and characteristic X-rays. SEM primarily utilizes SEs and BSEs for imaging. SEs are low-energy electrons emitted from the very surface of the sample, providing topographical information. BSEs are high-energy electrons from the incident beam that are scattered back from the sample elastically, providing compositional information based on atomic number contrast. It is especially useful for studying surface features such as grain boundaries, particle size, and texture.

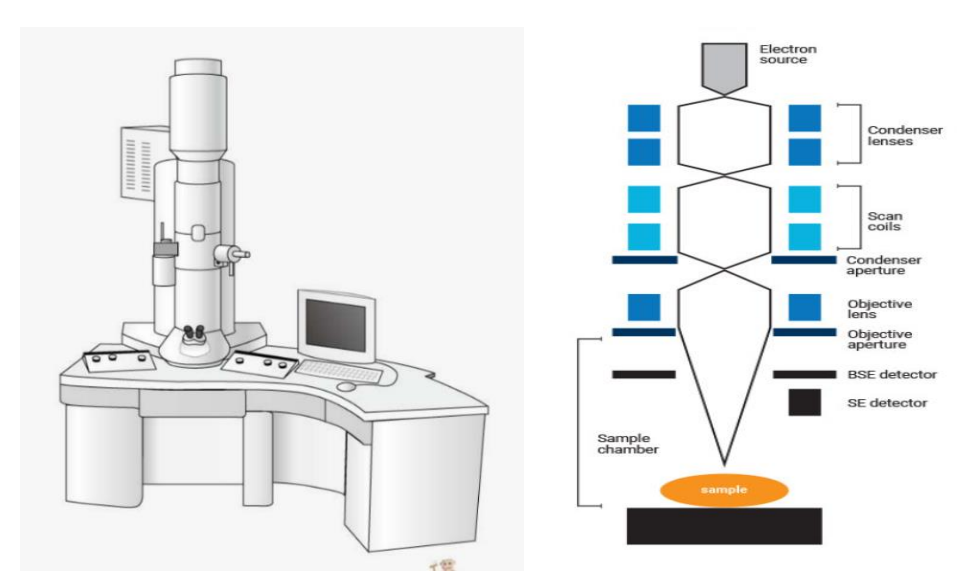


Fig. 7: Diagrammatic representation of SEMss

3.2.3 Energy Dispersive X-ray Spectroscopy (EDS)

EDS is an analytical technique used for elemental analysis of a sample. It is typically coupled with SEM. Its principle is based on the generation of characteristic X-rays when the incident electron beam interacts with the atoms in the sample. When a high-energy electron beam strikes an atom, it can eject an inner-shell electron, creating a vacancy. An electron from a higher energy shell then drops into this

10



vacancy to fill it, releasing the excess energy as a characteristic X-ray photon, whose energy is unique to the element from which it originated. EDS provides qualitative and semi-quantitative elemental analysis of the sample. It helps in determining the elemental composition of elements within a sample.

3.2.4 Transmission Electron Microscopy (TEM)

TEM is a powerful characterization technique that uses a beam of electrons transmitted through an ultra-thin sample to obtain high-resolution images, diffraction patterns, and elemental information. Unlike SEM, which images the surface, TEM provides internal structural and morphological information. The principle relies on the wave-particle duality of electrons, a high-energy electron beam (with a very short wavelength) can be transmitted through a sample, and the interaction of these electrons with the sample structure provides information about its internal morphology, crystal structure, and defects. TEM provides detailed internal structural information at atomic to nanometer resolution, including crystal structure, lattice defects, grain boundaries, and morphology. It is suitable for both imaging and diffraction studies.

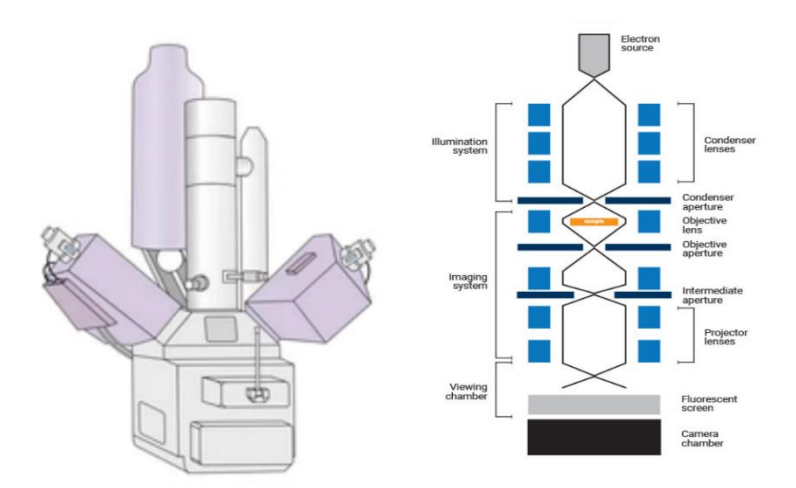


Fig. 8: Diagrammatic Representation of TEM

3.2.5 Selected Area Electron Diffraction (SAED)

SAED is a technique performed within a TEM to obtain crystallographic information from a specific, small region of a thin sample. Its basic principle is based on the diffraction of electrons by the periodic atomic planes within a crystalline material. Similar to XRD, constructive interference occurs when xix



electrons are scattered by atomic planes. However, due to the much shorter wavelength of electrons compared to X-rays, the diffraction angles are much smaller, and the diffraction pattern consists of spots or rings rather than continuous peaks. SAED provides insights on the crystal structure and phase identification of materials. It is particularly useful in identifying crystalline phases and analysing polycrystalline or nanocrystalline samples.

3.3 Electrode Fabrication

The working electrode was fabricated using composite of Active material (AM), Activated Carbon (AC), along with Polyvinylidene Fluoride (PVDF) as binder in a ratio of 8:1:1 ratio. The components were thoroughly mixed in N-methyl Pyrrolidone (NMP) solvent to form a homogeneous slurry. This slurry was uniformly coated on Cu foil (current collector) using doctor blade and dried at 120°C for 12 hours to ensure complete evaporation of the solvent and proper adhesion of the electrode material. After drying, circular electrodes of 16 mm diameter were punched out from the coated foil. These electrodes were then assembled into coin cells inside an argon-filled glove box workstation (MBraun) with O2 and H2O level below 0.5 ppm to prevent contamination. A coil cell of standard CR2016 configuration with 20 diameter and 1.6 mm thickness was used for assembling. A lithium metal chip was used as both the reference and counter electrode. A Celgard 2400 separator (Polypropylene membrane) was placed between working and lithium chip to prevent short-circuiting while allowing ionic conductivity. The electrolyte employed in the cells was 1M LiFePO4 in organic solvent EC DMC in 1:1, by volume ratio. Additionally, a metal spacer was inserted to accommodate any excess internal space and ensure firm contact between components.





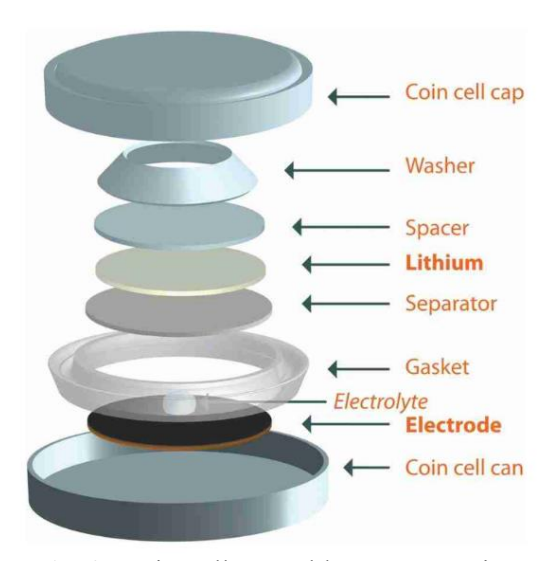


Fig. 9: Coin-cell assembly representation

3.4 Electrochemical Measurement

Electrochemical techniques are a category of analytical methods that utilize electrochemical principles to analyze and examine chemical reactions, investigate substance's properties, and determine concentrations. Electrochemical techniques present more benefits than technologies of surface modification. The electrochemical methods consist of measurements, Electrochemical Impendence Spectroscopy (EIS), Cyclic Voltammetry (CV), and Galvanostatic Charge/Dis-charge. In this work, the EIS and CV measurements were performed by BioLogic Potentiostat and software EC Lab. The GCD characteristics were evaluated by Lithium-Ion Battery Cycler system.

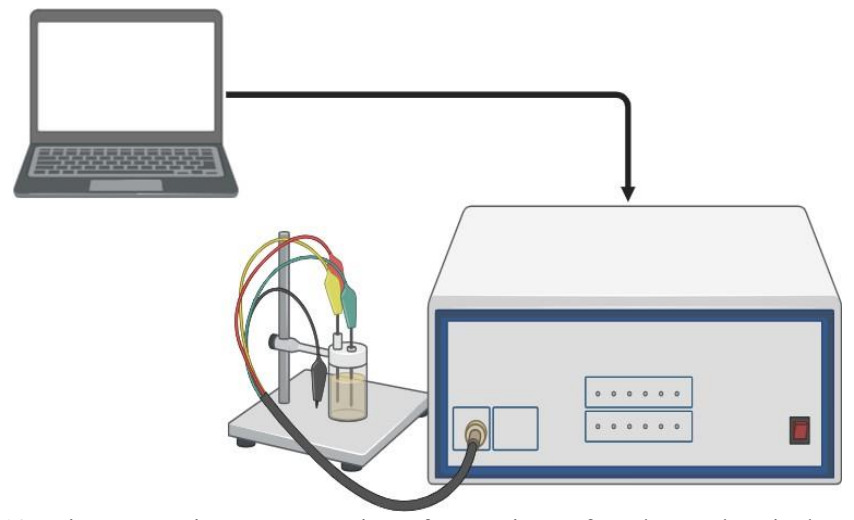


Fig. 10: Diagrammatic Representation of Potentiostat for Electrochemical analysis

3.4.1 Electrochemical Impendence Spectroscopy (EIS)

xxi



EIS is a technique employed to investigate the electrochemical properties of material by using a small AC voltage and measuring the resultant AC current over low and high frequencies. The fundamental principle involves disturbing an system from its equilibrium state with a sinusoidal potential and analysing the response as a function of frequency. The impedance gives information about the processes occurring at the electrode-electrolyte interface, including charge transfer kinetics, solution resistance, and lithium-ion diffusion coefficient. EIS data are primarily visualized through Nyquist and Bode plots, which are subsequently analysed using equivalent circuit modelling.

3.4.2 Cyclic Voltammetry (CV)

CV analysis investigates the redox behaviour and reaction kinetics of electroactive species by sweeping the potential of the working electrode linearly within potential window at a constant scan rate, while simultaneously measuring the resultant current. The principle involves employing a potential waveform to the electrode, causing the potential to sweep in one direction (anodic scan) and then reverse and sweep back in the reverse direction (cathodic scan). As the potential is swept, electroactive species at the electrode surface undergo oxidation or reduction, leading to characteristic current responses. The shape and position of the resulting current-potential peaks provide information about reaction reversibility, reaction mechanisms, and diffusion processes. The area under the CV curve can be correlated with the specific capacitance of the electrode material.

3.4.3 Galvanostatic Charge/Dis-charge (GCD)

GCD is an electrochemical method employed to evaluate the capacity and cycling stability of energy storage devices. The principle involves applying a constant current to the cell and monitoring the resultant potential response as a function of time. During charge, a constant positive current is applied, resulting in potential increases, while during discharge, a constant negative current is applied, and the resulting potential decreases. The shape of the voltage profile gives information about the charge storage mechanism of the device.

12

xxii



Chapter 4

RESULTS AND DISCUSSIONS

4.1 Phase Analysis

The NMO phase was confirmed through XRD analysis as shown in Fig.11, revealing the cubic lattice and Fd3m space group, perfectly matching with JCPDS 01-071-0852. The reflections (111), (220), (311), (222), (400), (422), (511), (440), (531), (622), (444), and (731) corresponding to NMO. The sharp and well-defined peaks indicate that the synthesised material possesses high crystallinity and it may result with enhanced structural stability during electrochemical reactions. The W-H plot and Scherrer's equation both were employed to calculate the crystallite size of the synthesised sample (Fig. 12). The W-H plot gives a negative slope indicating that there is a lattice compression within the material.

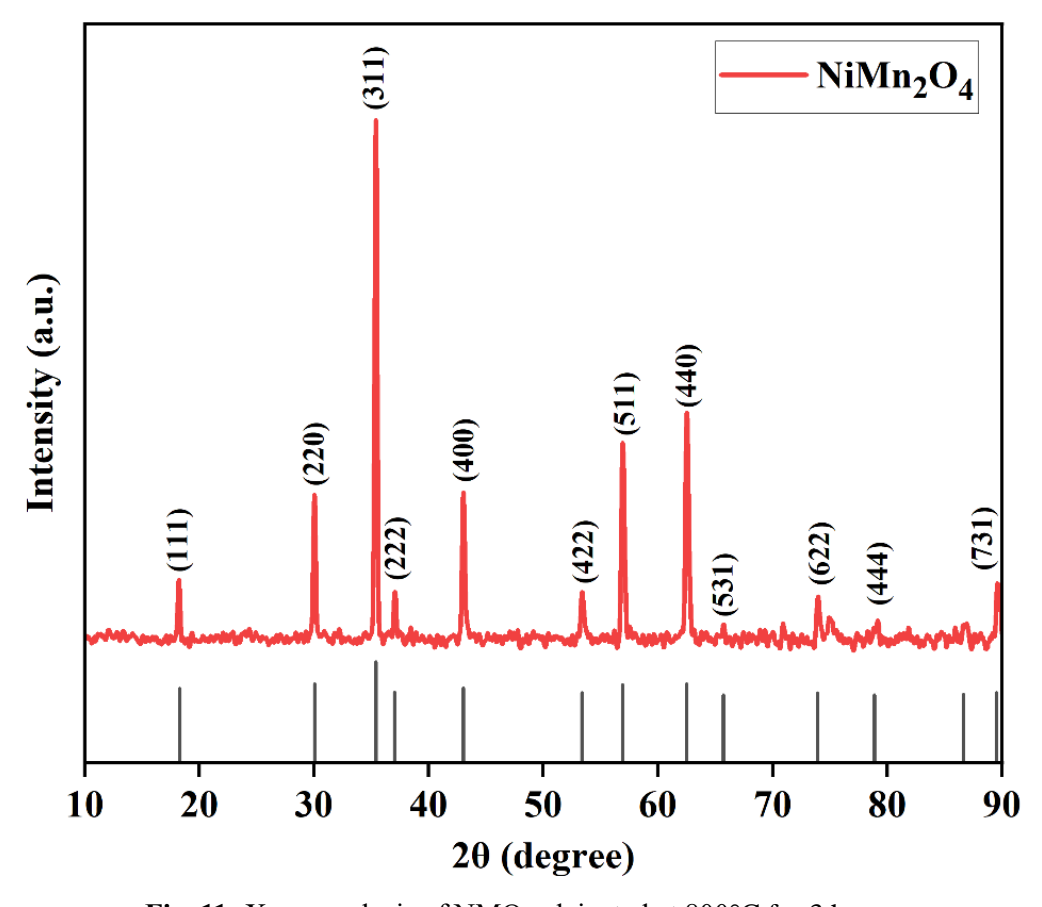


Fig. 11: X-ray analysis of NMO calcinated at 800°C for 3 hours.



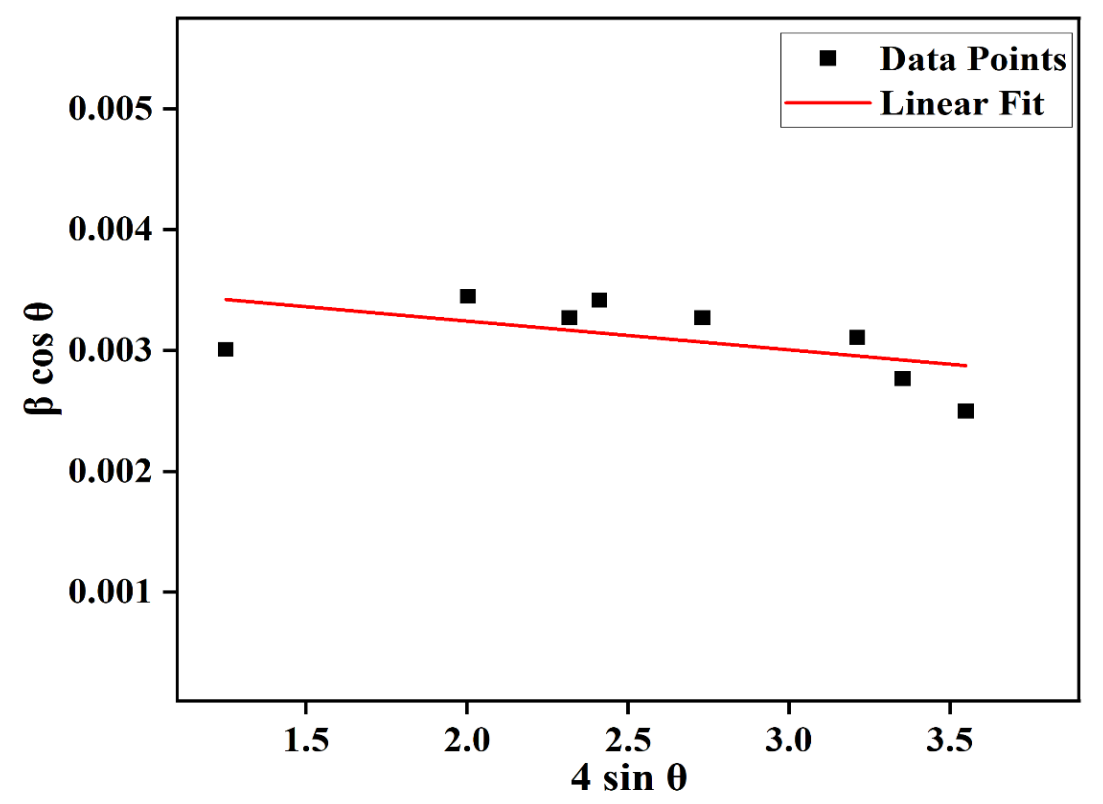


Fig. 12: Williamson-Hall (W-H) plot of synthesised sample

4.2 Morphological Analysis

The morphology and particle size of the synthesised NMO were thoroughly investigated using SEM and TEM analysis. The SEM images, presented in Figure 13, reveal the overall architecture, particle size, and surface characteristics of the synthesized NMO material. As shown in Fig. 13 (a-b), the material exhibits a relatively uniform morphology, primarily composed of hexagonal shape. The average particle size is estimated to be approximately 282.32 nm, with a size range observed between 250 to 350 nm. At higher magnification, as seen in Fig. 13 c), the individual particle surface appears as a proper hexagon shaped, and distinct inter-particle voids are visible, contributing to the overall porosity of the material. This observed morphology is crucial for indicating the material's electrochemical performance. The extent of porosity and voids facilitates the diffusion of lithium ions through the electrode material, thereby reducing diffusion pathways and potentially enhancing the material's rate capability. The overall architecture appears to provide sufficient connectivity for efficient electron transport within the electrode.



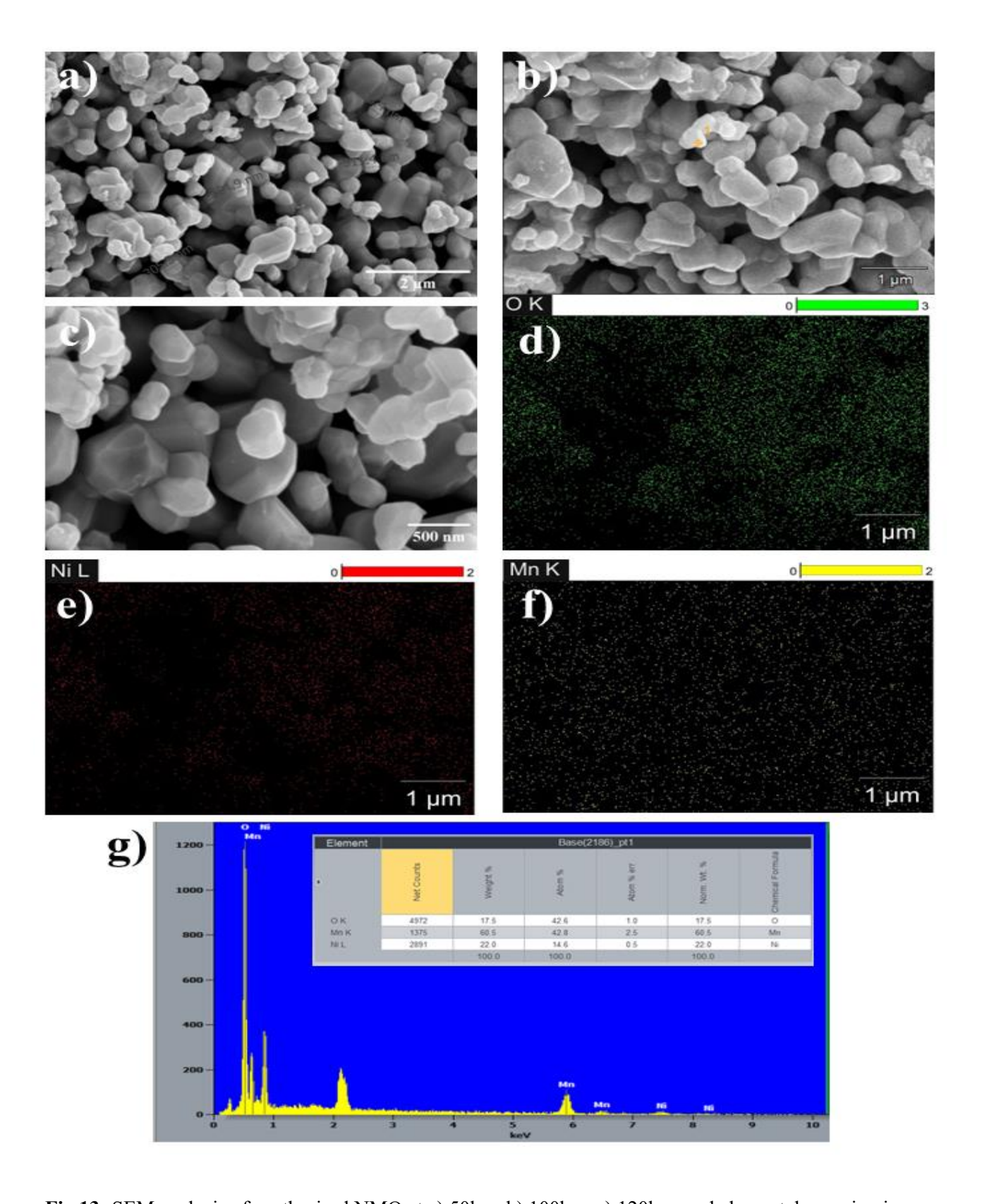


Fig 13: SEM analysis of synthesised NMO at a) 50k x, b) 100k x, c) 120k x, and elemental mapping images of d) Oxygen (green), e) Nickel (red), f) Manganese (yellow) and g) EDS analysis along with map sum spectrum

XXV





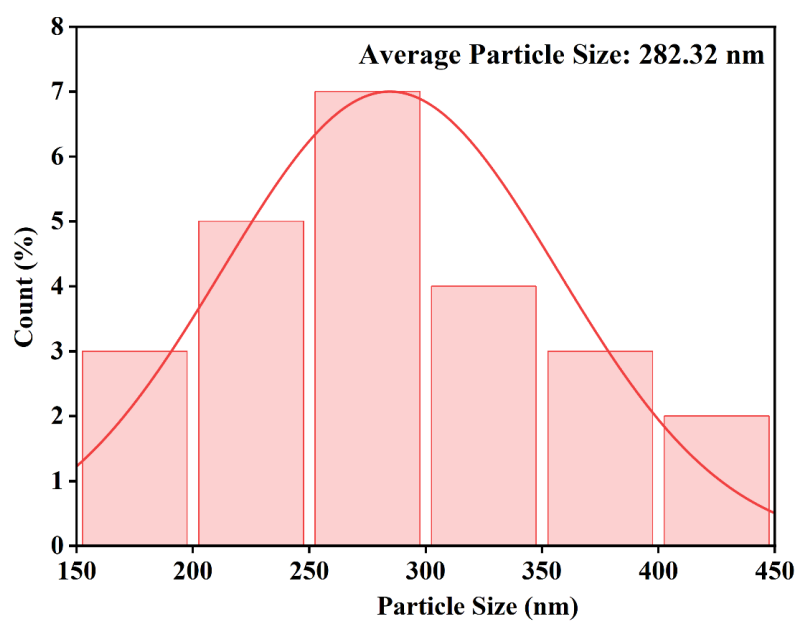


Fig 14: SEM histogram for average particle size

TEM analysis (Fig. 4 (a,b)) confirmed the hexagonal morphology and revealed a smaller average particle size of 180.52 nm. Fig. 4(a-c) shows the TEM results of NMO particles at different magnification along with SAED pattern. The crystalline structure of the NMO particles was investigated using both XRD and SAED pattern respectively. The d-spacing calculated from the SAED pattern were found to be in excellent agreement with the d-spacings obtained from the XRD data with matching the lattice planes. This strong correlation confirms that the NMO possess the expected crystalline phase. Despite confirming the correct phase and consistent d-spacing.

Morphological analysis conducted using SEM revealed that the as-synthesized nanoparticles have an average particle size of approximately 282.32 nm. However, TEM analysis, which involved a more vigorous dispersion step, showed a smaller average particle size of 186 nm. This discrepancy is commonly observed and suggests that while the primary particles are indeed around 180.52 nm, they exhibit a tendency to form loosely bound agglomerates or aggregates in their dry state, which are captured by SEM at the larger 282 nm scale. SEM, TEM analysis describes uniform microscale particles that directly supports the lithium-ion diffusion pathways and increased electrode-electrolyte contact area, thereby positively influencing the material's electrochemical performance. The

xxvi



morphological analysis has been added in the revised manuscript with "RED" text as separate subsection in results and discussions. The observed crystalline size and particle size along with observed porosity directly supports improved lithium-ion diffusion pathways and increased electrode-electrolyte contact are, thereby influencing charge storage capability of NMO as an anode.

Fig 15: TEM analysis of NMO at a) 200nm, b) 50 nm, and c) SAED analysis at 2 nm range

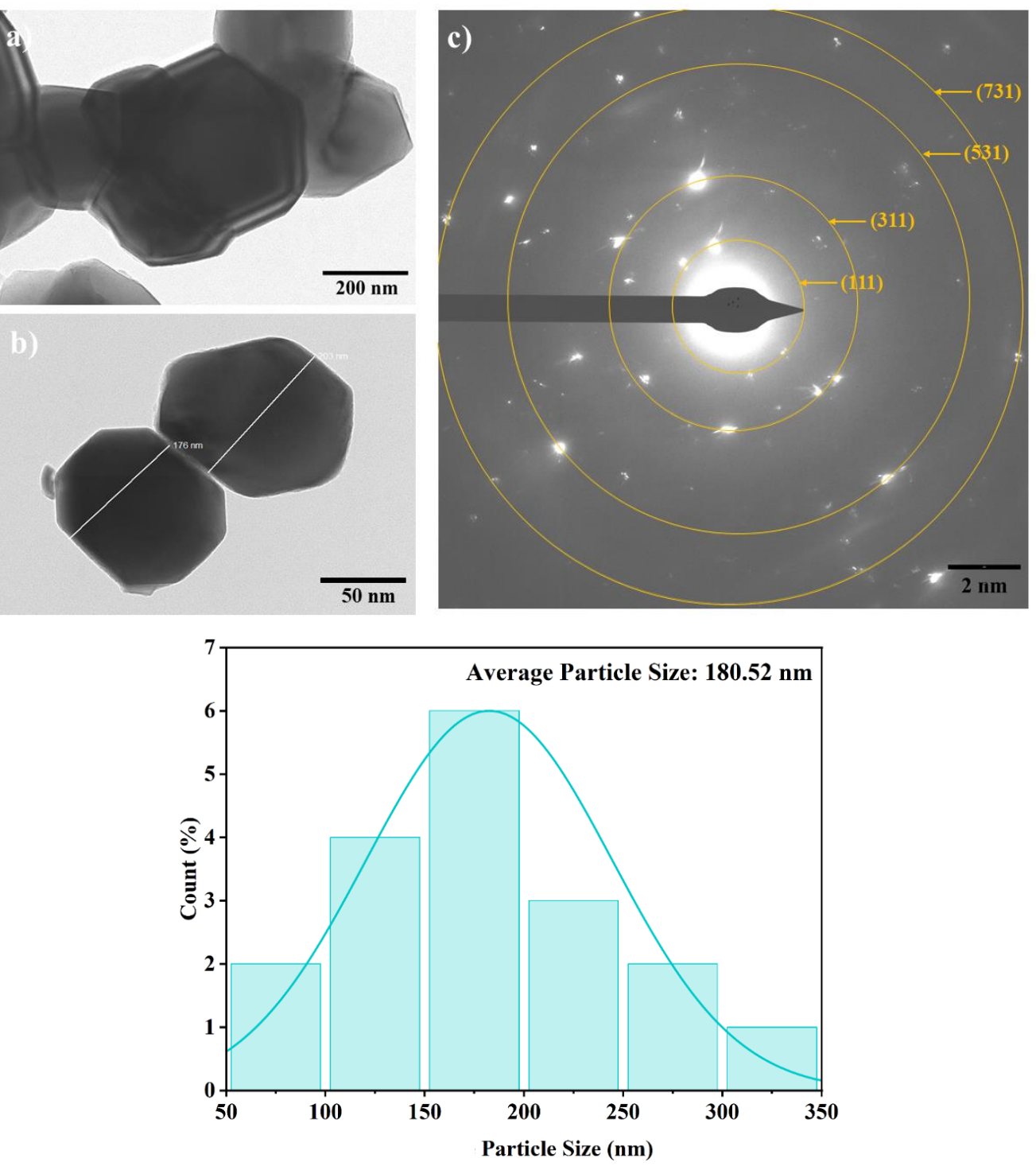


Fig 16: TEM histogram for average particle size xxvii





4.3 Electrochemical Analysis

The lithium-ion diffusion coefficient is calculated through two techniques, EIS and CV. Since, both the techniques are used to calculate Li⁺ diffusion coefficient but their underlying principles differs. EIS uses an AC voltage to probe impedance across a range of frequencies. In the low frequency region, diffusion appears as a Warburg impedance, characterized by a linear region in the Nyquist plot. Whereas, the CV involves sweeping a voltage and measuring corresponding current. The peak currents in the anodic and cathodic region are diffusion-limited and are directly related to Li⁺ diffusion coefficient. Hence, both of these techniques are employed in this research work to study the Li⁺ diffusion coefficient of the synthesised material.

4.3.1 EIS analysis

35

27

EIS tests are conducted to investigate the reactions taking place on the electrode surface during electrochemical processes. Fig. 5 shows the Nyquist plot of NMO as an anode measured at 5mV AC amplitude, between the frequency interval of 1 MHz to 100 Hz at 5 mV AC amplitude. To measure the ionic conductivity, following relation (12) has been used:

$$\sigma = \frac{t}{R_* \Delta} \tag{12}$$

where, σ, R, t, and A represents conductivity, bulk resistance, thickness and surface area of electrode, respectively.

In Nyquist plot, it is observed that in the high- frequency region, there is a semi-circle showing resistance and in low- frequency domain, a straight line corresponding to the Warburg impedance. The circuit fitting was done using EIS spectrum analyser software. The data were fitted using an appropriate equivalent circuit model. The Warburg Coefficient (σ_W) was obtained from the slope of the real part of the impedance (Z') versus the inverse square root of frequency in the low-frequency

Page 34 of 45 - Integrity Submission

xxviii



region. The Li⁺ diffusion coefficient is evaluated by Warburg coefficient with the help of following equation (13):

$$D_{L} = \left(\frac{0.5 R^{2} T^{2}}{n^{2} * F^{2} * A^{2} * \sigma w^{2} * C_{L}^{2}}\right)$$
(13)

where, D_L , R, T, F, n, A, σ_w , and C_L represents lithium-ion diffusion coefficient, gas constant, absolute temperature (in K), Faraday constant, no. of electrons involved, surface area of the electrode, Warburg coefficient, and concentration of lithium, respectively. The lithium-ion diffusion was observed to be around 10^{-14} cm² s⁻¹.

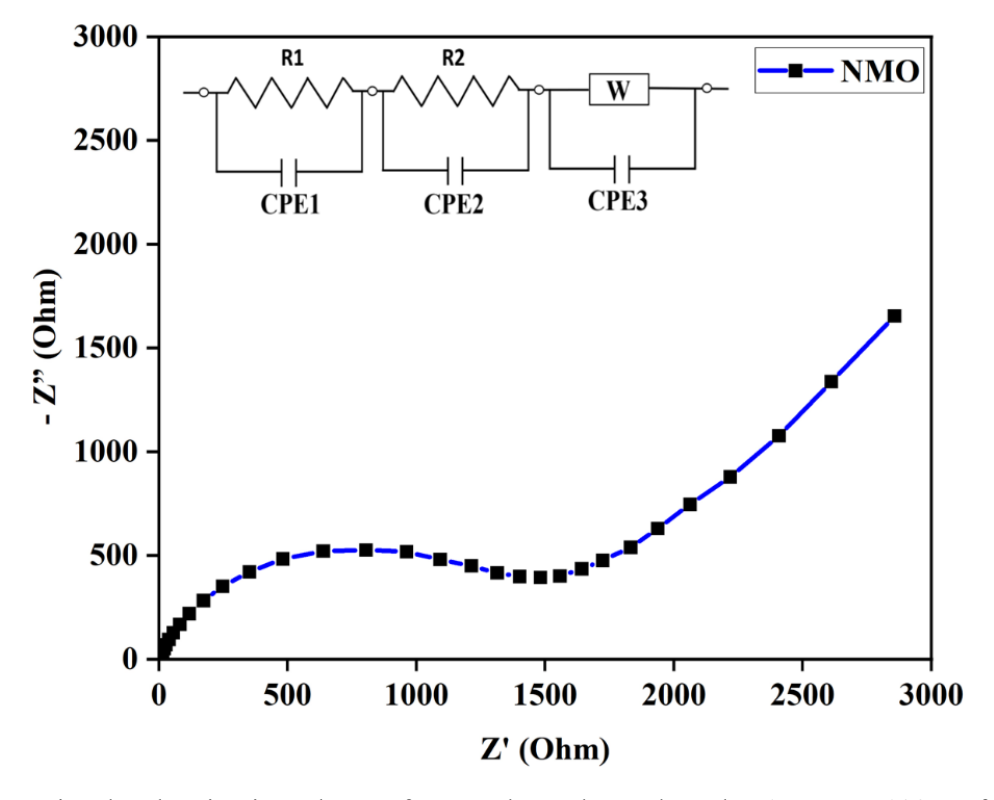


Fig. 17: Nyquist plot showing impedance of NMO electrode conducted at 1 MHz to 100 Hz frequency range and 5 mV AC amplitude.

4.3.2 CV analysis

To further analyse the diffusion coefficient more precisely CV analysis has been done. Fig. 6 shows the CV results of synthesised NMO for 3 cycles at 0.1mV s⁻¹ scan rate and potential window between 0 V to 3V. The first cathodic scan shows peak around 0.3 V - 0.5 V, attributes to the reduction of



NiMn₂O₄ to metallic Nickel and Manganese and formation of Li₂O as shown in equation (7). The subsequent anodic scan, revealed a broad oxidation peak around 0.8 – 1.8 V, attributed to Ni and Mn oxidation as their reaction with Li₂O as shown in reaction (8) and (9), consistent with the overall conversion reaction happens in NMO as an anode material.

The specific capacitance is estimated by using the equation (14):

$$C_{p} = \frac{A}{2mK(v_{2}-v_{1})} \tag{14}$$

where, C_p , A, K, and (v_2-v_1) represents specific capacitance, surface area, mass, scan rate and potential window, respectively. The specific capacitance of NMO was found to be 290.05 F g⁻¹.

The Randles-Ševčík equation (15) was employed to calculate the diffusion coefficient of Li⁺ ions:

$$I_p = 2.69 \times 10^5 * n^{3/2} * A * C_L * \sqrt{D_L} * \sqrt{K}$$
 (15)

$$D_{L} = \left(\frac{I_{P}}{2.69 \times 10^{5} *A* n^{3} *C_{L} *K^{1/2}}\right)^{2}$$
(16)

where, D_L , I_p , K, n, C_L , and A denotes the lithium-ion diffusion coefficient, anodic and cathodic peak current, scan rate, number of electrons involved, concentration of lithium ions, and surface area, respectively. The lithium-ion diffusion coefficient was found to be $10^{-13} - 10^{-14}$ cm² s⁻¹. The derived D_L from EIS closely matches with the values obtained through CV analysis, reinforcing the consistency of the diffusion mechanism in NMO using Warburg impedance of the Nyquist plot.



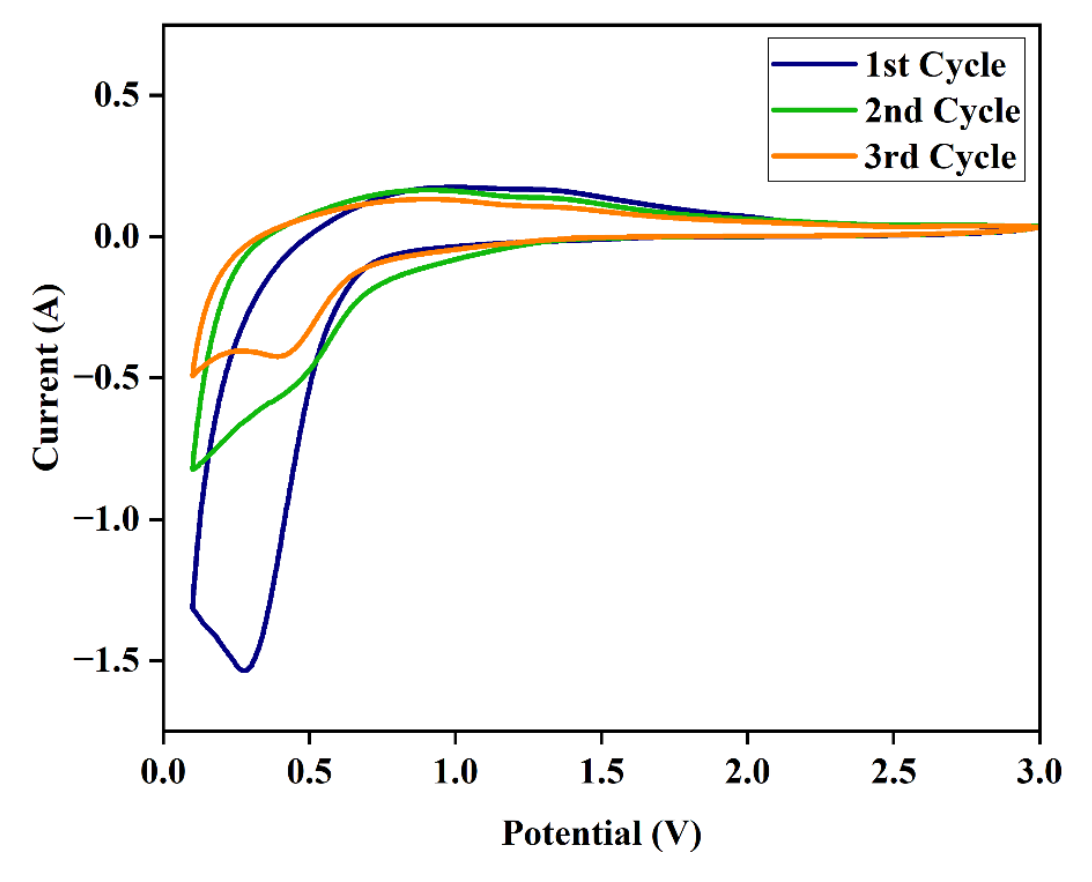


Fig. 18: Cyclic voltammetry curves of synthesised NMO material obtained at 0.1 mV s⁻¹ scan rate.

4.3.3 GCD analysis

Further, specific capacitance along with charge/dis-charge behaviour NMO electrode is also calculated using GCD technique. Figure 7 shows the GCD curves indicating lithium-ion storage behaviour during charge/ dis-charge cycle. At 0.01 C-rate, the half-cell was employed, allowing for first dis-charge and followed by further cycles to observe behaviour over time. The redox peaks observed in CV correspond well with the voltage plateaus in the GCD profile, affirming the reversibility of the redox processes. The peak in the CV curves near 0.3 - 0.5 V matches with this discharge plateau in GCD appears in 0.6 - 0.3 V. This indicates the same electrochemical process is responsible for both features, confirming consistent behaviour across both techniques. The specific capacitance of the electrode has been measured using given formula (17):

$$C_{P} = \frac{I_{m} * \Delta t}{\Delta v} \tag{17}$$

xxxi

28

where, C_p , I_m , Δt , and Δv represents specific capacitance, current density, discharge time, and potential window, respectively.

Moreover, the specific capacitance values calculated from GCD were found to be in good agreement with those obtained via CV, supporting the validity of the electrochemical performance.

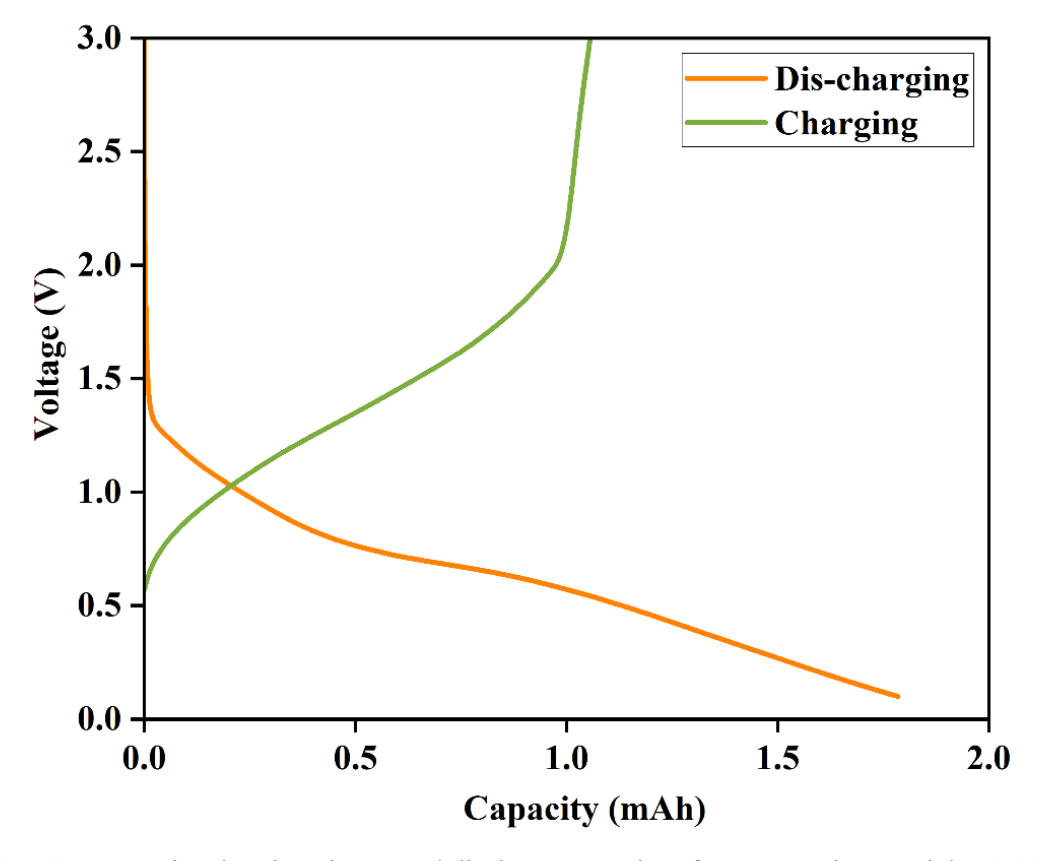


Fig. 19: GCD plot showing charge and discharge capacity of NMO anode material at 0.01C-rate.

xxxii



Chapter 5 CONCLUSIONS

5.1 Conclusions

The NMO has been synthesized using a simple solid-state reaction method. The XRD results revealed that prepared sample crystallizes in a cubic structure of Fd3m space group, and it matches perfectly with the standard database file no. JCPDS 01-071-0852. The crystallite size was determined by Scherrer's equation and W-H plot and was found to be \sim 34 nm. The SEM and TEM analysis confirms the hexagonal-shape morphology and polycrystalline nature. The particle size evaluated with SEM was found to be 282.32 nm and with TEM was around 180.52 nm. The SAED results correlates with the XRD data for (111), (311), (531), and (731) lattice planes. The ionic conductivity of synthesised electrode was \sim 1.32 x 10^{-3} S cm $^{-1}$. The lithium-ion diffusion coefficient (DLi) for the half-cell, as determined by CV ranged from 10^{-13} to 10^{-14} cm 2 s $^{-1}$, while EIS measurements from Warburg impedance yielded values around 10^{-14} cm 2 s $^{-1}$. Also, the specific capacitance is around 290.02 F g $^{-1}$, which was analysed and correlated using CV and GCD plots.

5.2 Future Scopes

Further research will focus on synthesizing NMO@MoS2 composites to enhance Li+ diffusion kinetics. Subsequent Cu-doping of the NMO@MoS2 within this composite will further optimize ion transport and electrode stability. Comprehensive electrochemical analyses will precisely quantify the improved diffusion coefficients in these advanced structures. This work aims to establish a clear correlation between material modification and enhanced Li+ diffusion for superior battery performance.



REFERENCES

- 1. Palacin, M. R.: Recent advances in rechargeable battery materials: a chemist's perspective. *Chemical Society Reviews*, 38(9), 2565-2575, (2009).
- Fichtner, M., Edström, K., Ayerbe, E., Berecibar, M., Bhowmik, A., Castelli, IE., Clark, S., Dominko, R., Erakca, M., Franco, A., and Grimaud, A.: Rechargeable batteries of the future—the state of the art from a BATTERY 2030+ perspective. Advanced Energy Materials, 12(17), 2102904, (2022).
- 3. Bode, H. Lead-acid batteries (1977).
- 4. Lopes, P. P. and Stamenkovic, V. R.: Past, present, and future of lead-acid batteries. Science, 369(6506), 923-924, (2020).
- 5. Lach, J., Wróbel, K., Wróbel, J., Podsadni, P., and Czerwiński, A.: **Applications of carbon in lead-acid batteries: a review**. *Journal of Solid State Electrochemistry*, *23*, 693-705 (2019).
- 6. Petrovic, S., and Petrovic, S.: Nickel-cadmium batteries. *Battery Technology Crash Course: A Concise Introduction*, 73-88 (2021).
- Galushkin, N. E., Yazvinskaya, N. N., and Galushkin, D. N. Nickel-cadmium batteries with pocket electrodes as hydrogen energy storage units of high-capacity. *Journal of Energy Storage*, 39, 102597, (2021).
- 8. McDowall, J. Nickel-cadmium batteries for energy storage applications. In Fourteenth Annual Battery Conference on Applications and Advances. Proceedings of the Conference (Cat. No. 99TH8371) 303-308, IEEE (1999).
- 9. Taniguchi, A., Fujioka, N., Ikoma, M., and Ohta, A.: **Development of nickel/metal-hydride batteries for EVs and HEVs**. *Journal of power sources*, *100*(1-2), 117-124, (2001).
- Arun, V., Kannan, R., Ramesh, S., Vijayakumar, M., Raghavendran, P. S., Siva Ramkumar, M., Anbarasu,
 P., and Sundramurthy, V. P.: Review on li-ion battery vs nickel metal hydride battery in EV. Advances in Materials Science and Engineering, 2022(1), 7910072, (2022).
- 11. Li, M., Lu, J., Chen, Z., and Amine, K.: **30 years of lithium-ion batteries**. *Advanced materials*, *30*(33), 1800561, (2018).
- 12. Kim, T., Song, W., Son, D. Y., Ono, L. K., and Qi, Y.: Lithium-ion batteries: outlook on present, future, and hybridized technologies. *Journal of materials chemistry A*, 7(7), 2942-2964, (2019).
- 13. Manthiram, A.: An outlook on lithium ion battery technology. ACS central science, 3(10), 1063-1069, (2017).





- 14. Bruce, P. G., Hardwick, L. J., and Abraham, K. M.: Lithium-air and lithium-sulfur batteries. MRS bulletin, 36(7), 506-512, (2011).
- 15. Kurzweil, P.: Lithium battery energy storage: State of the art including lithium–air & lithium–sulfur systems. Electrochemical energy storage for renewable sources and grid balancing, 269-307, (2015).
- 16. Li, J., Daniel, C., and Wood, D.: Materials processing for lithium-ion batteries. *Journal of Power Sources*, 196(5), 2452-2460, (2011).
- 17. Blomgren, G. E.: **The development and future of lithium ion batteries**. *Journal of The Electrochemical Society*, *164*(1), A5019, (2016).
- 18. Scrosati, B., Hassoun, J., and Sun, Y. K.: Lithium-ion batteries. A look into the future. *Energy & Environmental Science*, 4(9), 3287-3295, (2011).
- 19. Jow, T. R., Xu, K., Borodin, O., and Ue, M. (Eds.).: Electrolytes for lithium and lithium-ion batteries 58, *New York: Springer* (2014).
- 20. Xu, K.: Electrolytes and interphases in Li-ion batteries and beyond. *Chemical reviews*, 114(23), 11503-11618, (2014).
- 21. Wang, C., Yu, L., Fan, W., Liu, J., Ouyang, L., Yang, L., and Zhu, M.: Lithium difluorophosphate as a promising electrolyte lithium additive for high-voltage lithium-ion batteries. *ACS applied energy materials*, *1*(6), 2647-2656, (2018).
- 22. Pham, H. Q., Lee, H. Y., Hwang, E. H., Kwon, Y. G., and Song, S. W.: Non-flammable organic liquid electrolyte for high-safety and high-energy density Li-ion batteries. *Journal of power sources*, 404, 13-19, (2018).
- 23. Haregewoin, A. M., Wotango, A. S., and Hwang, B. J.: Electrolyte additives for lithium ion battery electrodes: progress and perspectives. *Energy & Environmental Science*, 9(6), 1955-1988, (2016).
- 24. Manthiram, A.: A reflection on lithium-ion battery cathode chemistry. *Nature communications*, 11(1), 1550, (2020).
- 25. Lyu, Y., Wu, X., Wang, K., Feng, Z., Cheng, T., Liu, Y., Wang, M., Chen, R., Xu, L., Zhou, J., Lu, Y., and Guo, B.: An overview on the advances of LiCoO2 cathodes for lithium-ion batteries. *Advanced Energy Materials*, 11(2), 2000982, (2021).
- 26. Radzi, Z. I., Arifin, K. H., Kufian, M. Z., Balakrishnan, V., Raihan, S. R. S., Abd Rahim, N., and Subramaniam, R.: Review of spinel LiMn2O4 cathode materials under high cut-off voltage in lithiumion batteries: Challenges and strategies. *Journal of Electroanalytical Chemistry*, 920, 116623, (2022).





- 27. Li, T., Chang, K., Hashem, A.M., Abdel-Ghany, A.E., El-Tawil, R.S., Wang, H., El-Mounayri, H., Tovar, A., Zhu, L., and Julien, C.M.: Structural and electrochemical properties of the high Ni content spinel LiNiMnO4. *Electrochem*, 2(1), 95-117 (2021).
- 28. Chen, S. P., Lv, D., Chen, J., Zhang, Y. H., and Shi, F. N.: Review on defects and modification methods of LiFePO4 cathode material for lithium-ion batteries. *Energy & Fuels*, *36*(3), 1232-1251, (2022).
- 29. Yu, H., and Zhou, H.: **High-energy cathode materials (Li2MnO3–LiMO2) for lithium-ion batteries.** *The journal of physical chemistry letters*, *4*(8), 1268-1280 (2013).
- 30. Välikangas, J., Laine, P., Hietaniemi, M., Hu, T., Tynjälä, P., and Lassi, U.: **Precipitation and calcination** of high-capacity LiNiO2 cathode material for lithium-ion batteries. *Applied sciences*, 10(24),8988, (2020).
- 31. Liu, Z., Jiang, Y., Hu, Q., Guo, S., Yu, L., Li, Q., Liu, Q., and Hu, X.: Safer lithium-ion batteries from the separator aspect: development and future perspectives. *Energy & Environmental Materials*, 4(3), 336-362, (2021).
- 32. He, S., Huang, S., Wang, S., Mizota, I., Liu, X., and Hou, X.: Considering critical factors of silicon/graphite anode materials for practical high-energy lithium-ion battery applications. *Energy & Fuels*, 35(2), 944-964, (2020).
- 33. Zhang, C., Wang, F., Han, J., Bai, S., Tan, J., Liu, J., and Li, F.: Challenges and recent progress on silicon-based anode materials for next-generation lithium-ion batteries. *Small Structures*, 2(6), 2100009, (2021).
- 34. Julien, C. M., and Mauger, A.: Fabrication of Li4Ti5O12 (LTO) as anode material for Li-Ion batteries. *Micromachines*, 15(3), 310, (2024).
- 35. Cheng, X., Tang, C., Yan, C., Du, J., Chen, A., Liu, X., ... & Zhang, Q. (2023). Preparation of porous carbon spheres and their application as anode materials for lithium-ion batteries: A review. *Materials Today Nano*, 22, 100321, (2023).
- 36. De las Casas, C., and Li, W.: A review of application of carbon nanotubes for lithium ion battery anode material. *Journal of Power Sources*, 208, 74-85, (2012).
- 37. Yamamura, H., Nobuhara, K., Nakanishi, S., Iba, H., and Okada, S.: Investigation of the irreversible reaction mechanism and the reactive trigger on SiO anode material for lithium-ion battery. *Journal of the Ceramic Society of Japan*, 119(1395), 855-860, (2011).





- 38. Zhu, J., Ding, Y., Ma, Z., Tang, W., Chen, X., and Lu, Y.: Recent progress on nanostructured transition metal oxides as anode materials for lithium-ion batteries. *Journal of Electronic Materials*, *51*(7), 3391-3417, (2022).
- 39. Korthauer, R.: Lithium-ion batteries: basics and applications. Springer (2018).
- 40. Colclasure, A. M., and Kee, R. J.: Thermodynamically consistent modeling of elementary electrochemistry in lithium-ion batteries. *Electrochimica Acta*, 55(28), 8960-8973 (2010).
- 41. Zhao, L., Ding, B., Qin, X. Y., Wang, Z., Lv, W., He, Y. B., Yang, QH., Kang, F.: Revisiting the roles of natural graphite in ongoing lithium-ion batteries. *Advanced Materials*, *34*(18), 2106704, (2022).
- 42. Gulbinska, M. K.: Lithium-ion battery materials and engineering: current topics and problems from the manufacturing perspective. *Springer* (2014).
- 43. Gao, J., Shi, S. Q., and Li, H.: Brief overview of electrochemical potential in lithium ion batteries. *Chinese Physics B*, 25(1), 018210, (2015).
- 44. Zheng, G., Yang, Y., Cha, J. J., Hong, S. S., and Cui, Y.: Hollow carbon nanofiber-encapsulated sulfur cathodes for high specific capacity rechargeable lithium batteries. *Nano letters*, 11(10), 4462-4467, (2011).
- 45. Lee, H., Yang, S., Kim, S., Song, J., Park, J., Doh, C. H., ha, Y.C., Kwon, T.S., and Lee, Y. M.: Understanding the effects of diffusion coefficient and exchange current density on the electrochemical model of lithium-ion batteries. *Current Opinion in Electrochemistry*, 34, 100986, (2022).
- 46. Yu, P., Popov, B. N., Ritter, J. A., and White, R. E.: **Determination of the lithium ion diffusion coefficient** in graphite. *Journal of The Electrochemical Society*, *146*(1), 8, (1999).
- 47. Geng, Z., Chien, Y. C., Lacey, M. J., Thiringer, T., and Brandell, D.: Validity of solid-state Li+ diffusion coefficient estimation by electrochemical approaches for lithium-ion batteries. *Electrochimica Acta*, 404, 139727, (2022).
- 48. Prajapati, A. K., and Bhatnagar, A.: A review on anode materials for lithium/sodium-ion batteries. *Journal of Energy Chemistry*, 83, 509-540, (2023).
- 49. Wang, F., Yi, J., Wang, Y., Wang, C., Wang, J., and Xia, Y.: Graphite Intercalation Compounds (GICs):

 A New Type of Promising Anode Material for Lithium-Ion Batteries. Advanced Energy Materials, 4(2), (2014).
- 50. Wang, R., Sun, S., Xu, C., Cai, J., Gou, H., Zhang, X., and Wang, G.: The interface engineering and structure design of an alloying-type metal foil anode for lithium ion batteries: a review. *Materials horizons*, 11(4), 903-922, (2024).

turnitin



- 51. Lu, Y., Yu, L., and Lou, X. W. D. (2018). Nanostructured conversion-type anode materials for advanced lithium-ion batteries. *Chem*, 4(5), 972-996, (2018).
- 52. Zheng, M., Tang, H., Li, L., Hu, Q., Zhang, L., Xue, H., and Pang, H.: **Hierarchically nanostructured** transition metal oxides for lithium-ion batteries. *Advanced science*, *5*(3), 1700592, (2018).
- 53. Park, H., Kim, K., Jeong, K., Kang, J. S., Cho, H. H., Thirumalraj, B., Sung, Y.E., Han, H.N., Kim, J.H., Dunand, DC., and Choe, H.: Integrated porous cobalt oxide/cobalt anode with micro-and nano-pores for lithium ion battery. *Applied Surface Science*, 525, 146592, (2020).
- 54. Khalil, A., Lalia, B. S., and Hashaikeh, R.: Nickel oxide nanocrystals as a lithium-ion battery anode: structure-performance relationship. *Journal of Materials Science*, *51*, 6624-6638 (2016).
- 55. Lv, L., Peng, M., Wu, L., Dong, Y., You, G., Duan, Y., Yang, W., He, L., and Liu, X.: Progress in iron oxides based nanostructures for applications in energy storage. *Nanoscale Research Letters*, 16(1), 138, (2021).
- 56. Rajagopalan, K., Ramasubramanian, B., Velusamy, S., Ramakrishna, S., Kannan, A. M., Kaliyannan, M., & Kulandaivel, S.: Examining the economic and energy aspects of manganese oxide in Li-ion batteries. *Materials Circular Economy*, 4(1), 22, (2022).
- 57. Zhao, Y., Li, X., Yan, B., Xiong, D., Li, D., Lawes, S., and Sun, X.: Recent developments and understanding of novel mixed transition-metal oxides as anodes in lithium-ion batteries. *Advanced Energy Materials*, 6(8), 1502175 (2016).
- 58. Kommu, P., Jana, S., Singh, G. P., Dash, R., Gurjar, M. K., and Bhattacharyya, A. S.: Mixed transition metal oxides for electrochemical energy storage. In *Handbook of Emerging Materials for Sustainable Energy*, 129-145 (2024).
- 59. Nwakanma, O., and Ezema, F. I.: Recent Advances in Composites of Mixed Transition Metal Oxides and Graphene Oxide–Based Anode Materials for Lithium-Ion Batteries. *Graphene Oxide in Enhancing Energy Storage Devices*, 193-208, (2022).
- 60. Jain, A., Panwar, A. K., and Tyagi, P. K.: Synthesis, characterization, and electrochemical investigation of citric-acid assisted nickel manganese oxide as anode material. *MRS Advances*, 7(27), 584-590 (2022).
- 61. Zhao, S., Li, H., Jian, Z., Xing, Y., and Zhang, S.: Self-assembled hierarchical porous NiMn₂O₄ microspheres as high performance Li-ion battery anodes. RSC advances, 8(73), 41749-41755 (2018).





- 62. Kang, W., Tang, Y., Li, W., Yang, X., Xue, H., Yang, Q., and Lee, C. S.: High interfacial storage capability of porous NiMn 2 O 4/C hierarchical tremella-like nanostructures as the lithium ion battery anode. Nanoscale, 7(1), 225-231 (2015).
- 63. Li, L., Yao, Q., Liu, J., Ye, K., Liu, B., Liu, Z., Yang, H., Chen, Z., Duan, J. and Zhang, B.: Porous hollow superlattice NiMn2O4/NiCo2O4 mesocrystals as a highly reversible anode material for lithium-ion batteries. Frontiers in Chemistry, 6, 153 (2018).
- 64. Rajoba, S. J., Kale, R. D., Kulkarni, S. B., Parale, V. G., Patil, R., Olin, H., Park, H.H., Dhavale, R.P. and Phadatare, M.: Synthesis and electrochemical performance of mesoporous NiMn2O4 nanoparticles as an anode for lithium-ion battery. *Journal of Composites Science*, 5(3), 69 (2021).
- 65. Jain, A., Panwar, A. K., and Tyagi, P. K.: Preparation of NiMn2O4-NiMnO3@ MoS2 Nano-composites with Enhanced Electrochemical Performances for Lithium-ion Batteries. *Indian Journal of Engineering and Materials Sciences (IJEMS)*, 30(5), 689-693 (2023).
- 66. Han, M., Jia, H., Wang, Y., Li, S., and Liu, Y.: **High-performance NiMn2O4@ MXene nanocomposites** for aqueous zinc-ion battery. *Journal of Physics and Chemistry of Solids*, 196, 112411 (2025).
- 67. Lee, H., Yang, S., Kim, S., Song, J., Park, J., Doh, C. H., Ha, Y.C., Kwon, T.S. and Lee, Y.M.: Understanding the effects of diffusion coefficient and exchange current density on the electrochemical model of lithium-ion batteries. *Current Opinion in Electrochemistry*, 34,100986 (2022).
- 68. Ugata, Y., Motoki, C., Dokko, K., and Yabuuchi, N.: Fundamental methods of electrochemical characterization of Li insertion materials for battery researchers. *Journal of Solid State Electrochemistry*, 28(3), 1387-1401 (2024).
- 69. Manfo Theodore, A.: Structural, electrical, and electrochemical studies of the olivine LiMPO 4 (M= Fe, Co, Cr, Mn, V) as cathode materials for lithium-ion rechargeable batteries based on the intercalation principle. *Materials Open Research*, 2, 11, (2023).
- 70. Teotia, S., and Chaudhary, A.: Electrode Materials for High Energy Density Li-Ion. In Chemically Deposited Metal Chalcogenide-based Carbon Composites for Versatile Applications (pp. 215-243).

 Cham: Springer International Publishing, (2023).